Available online at https://link.springer.com/journal/42241
http://www.jhydrodynamics.com
Journal of Hydrodynamics, 2021, 33(3): 479-487
https://doi.org/10.1007/s42241-021-0054-4

Liutex force field model applied to three-dimensional flows around a circular cylinder at $Re = 3\,900$ *

Wei-wen Zhao[1], Chun-hui Ma[1], De-cheng Wan[1, 2], Yi-qian Wang[3]
1. *Computational Marine Hydrodynamics Lab (CMHL), School of Naval Architecture, Ocean and Civil Engineering, Shanghai Jiao Tong University, Shanghai 200240, China*
2. *Ocean College, Zhejiang University, Zhoushan 316021, China*
3. *School of Mathematical Science, Soochow University, Suzhou 215006, China*

(Received May 8, 2021, Revised June 7, 2021, Accepted June 8, 2021, Published online July 5, 2021)

Abstract: Recently, the Liutex-based force field models are proposed and applied to some two-dimensional flows to explore the possibility of direct vortex control strategies. In this paper, we applied the Liutex-based centripetal force model to three-dimensional flow around a circular cylinder at $Re = 3\,900$. The turbulent flows around the three-dimensional cylinder are modeled by the delayed detached-eddy simulations based on the two-equation k-ω shear stress transport (SST) model. The cylinder flow without adding the force field model is simulated in the first place. The statistical flow quantities are compared with experimental data to validate the accuracy of the current numerical models. Then the force field model is applied to the momentum equation in a specific control region near the cylinder to study the change of flow field and hydrodynamic performance. The effect of different control region locations with the same force field strength is discussed to find out the most influenced locations on the drag and lift. Based on the screened control region, the influence source term strength is further studied. Variations on the global statistical flow quantities, local instantaneous three-dimensional flow structures are analyzed and discussed. It is concluded that the Liutex-based force field model can effectively change the hydrodynamic behavior of flow past a cylinder and may provide a new direction for performance improvement and optimization.

Key words: Vortex manipulate, flow control, vortex shedding, Liutex vector

Introduction

In recent years, with the advancement of experimental and computational fluid dynamics, more and more researchers have been focusing on the analysis of vortex dynamics behaviors for flow around engineering structure[1]. The reason is that vortices represent the rotational effect of the flow field, and can directly impact the local pressure and hence change the overall hydrodynamic or aerodynamic performance of structures. For ocean engineering flows, for example, if the correlations between vortices and hydrodynamic performance have been determined and well understood, one can improve the hydrodynamic performance by altering the vortical structures in critical regions. This is conventionally achieved by adding some small structures on the surface of the original structure, or directly change the layout of the structures in the design phase. An example is the bilge keels which are commonly installed at the side bottom of hull surface for high-speed ships. When the ship performs roll motions, the bilge keels can generate vortices and damp the roll motions. In such a way, the roll motion performance of the ship is improved. From another perspective of view, we can control or manipulate vortices directly with the help of numerical tools in simulations. Numerical simulations of direct vortices control are easy to implement and may provide a new direction for the optimization design for engineering structures.

The direct control of the flow field requires a clear physical meaning of the vortex and an accurate and comprehensive vortex identification (VI) method. In the pioneering work of Liu et al.[2], the VI methods can be divided into three generations. Vorticity, defined as the curl of velocity, is categorized into the

* Projects supported by the National Natural Science Foundation of China (Grant Nos. 51909160, 51879159), the National Key Research and Development Program of China (Grant Nos. 2019YFB1704200, 2019YFC0312400).
Biography: Wei-wen Zhao (1990-), Male, Ph. D., Assistant Professor, E-mail: weiwen.zhao@sjtu.edu.cn
Corresponding author: De-cheng Wan, E-mail: dcwan@sjtu.edu.cn

first generation VI methods. Due to the weak correlations with vortex, vorticity is not able to represent vortical structures, especially in the near wall region for wall-bounded flows. To address this issue, several methods have been proposed, including Q, λ_2, Δ, λ_{ci} and other methods[3-7]. These methods are classified as the second generation VI methods. In most of these methods, a scalar with specified formulation is calculated from the velocity gradient and the vortical structures are represented by iso-surfaces extracted by arbitrarily chosen threshold values of the calculated scalar. The threshold value somewhat represents the swirling strength of vortices, but the physical meanings of these scalars are not clear. In addition, these methods more or less involve shear and stretch contamination problems which counts the shearing and stretching as a part of vortex strength. To overcome the above shortcomings, Liu et al.[8] proposed the concept of Liutex which is quite different from the previous first and second generation VI methods. Liutex is an eigenvalue-based method that is local, accurate, and unique[9]. It is defined as a vector, whose magnitude is the rotational strength of the fluid motion, and its direction is the local rotation axis of local fluid motions. Liutex could precisely describe the six core elements of vortex, namely, absolute strength, relative strength, local rotation axis, vortex rotation axis, vortex core size, and vortex boundary. Based on this definition, several methods including Liutex method, objective Liutex method[10], Liutex-Omega method[11-12], Liutex core line method[13] have been proposed. These Liutex-based methods are classified as the third generation VI methods.

Due to the comprehensive characteristics and clear physical meaning of Liutex for representing vortex, it is an ideal parameter to be used to construct a force field model for direct control the flow motions. In the pioneering work of Yu and Wang[14], they performed a preliminary study of direct vortex manipulation with the help of computational fluid dynamics (CFD). The objective is to obtain vortex dynamics after applying force field model and deduce vortex control strategies. They proposed two force field models based on Liutex, namely, the centripetal force field model and the counter-rotation force field model. The basic idea is to construct a source term based on the Liutex vector and add it into the Navier-Stokes equations. The two models can effectively reduce the vortex strength and eliminate the vortex structures. However, the implementation is very tricky. For instance, in the centripetal force model, the calculation of length scale requires the vortex core center which is difficult to find out for three-dimensional flows. In the counter-rotating model, a time scale is required to construct the source term. The time scale is determined according to some experience. Zhao et al.[15] simplified the Liutex-based centripetal force field model with a more general length scale formulation in the definition of source term and applied the model to a low Reynolds number two-dimensional cylinder flow at $Re = 100$. They discussed the influence of source term magnitude and control regions on the vortex dynamics of the cylinder flow.

In the present work, we extend the application of the force field model to a three dimensional cylinder flow with turbulent characteristics. The Reynolds number 3 900 is very representative for subcritical cylinder flow. It has been a classical test case for different turbulence modeling methods. Ma et al.[16] performed direct numerical simulation (DNS) of cylinder flow at $Re = 3\,900$. The mean velocity profiles and power spectra in both near wake and far downstream regions are in good agreement with experimental measurements. Studies based on large eddy simulations (LES) were also carried out by Moin et al.[17-18] and Parnaudeau et al.[19]. Moin's group is pioneer of LES studies for cylinder flow at $Re = 3\,900$. In their numerical studies, the mean velocity and Reynolds stress profiles are in good agreement with experimental data in the far wake region. They discussed the numerical dissipation of upwind and central differencing discretization schemes and found out the low-dissipation central differencing scheme gives more accurate power spectra of velocity at high wave numbers. However, their results show large discrepancy of velocity profile shapes in the near wake regions. This is believed to be attributed to the experimental error of the original data. In the paper published by Parnaudeau et al.[19], they not only performed LES simulations, but also conducted experimental investigations. The near wake region velocity profiles between numerical simulations and experimental measurements show no differences. Both are in good agreement with previous LES results of Kravochenko and Moin[18] and DNS results of Ma et al.[16]. Recent studies[20] also increase the confidence level of the experimental data from Parnaudeau et al.[16].

This paper is organized as follows, first the governing equations and centripetal force field model are briefly introduced, then the force field model is applied to the $Re = 3\,900$ cylinder flow, with different control regions and source term coefficients. Lift, drag, surface pressure and vortex structures are compared and discussed.

1. Governing equations for incompressible flow

The three-dimensional flow past a circular cylinder is treated as incompressible, unsteady, and

turbulent and is governed by the incompressible Navier-Stokes equations. Solving the equations directly requires very fine grid resolutions and huge computational costs. Instead of that, we employ the delayed detached-eddy simulation (DDES) and solve the DDES equations which is an averaged/filtered version of the original Navier-Stokes equations. By inserting the Liutex source term into the DDES equations, we obtained the final formulation which is given by

$$\frac{\partial \boldsymbol{u}}{\partial t} + (\boldsymbol{u}\cdot\nabla)\boldsymbol{u} = -\nabla\frac{p}{\rho} + \nabla\cdot(\nu_{\text{eff}}\nabla\boldsymbol{u}) + c\boldsymbol{a} \tag{1}$$

in which $\boldsymbol{u}$ and p are the averaged/filtered velocity and pressure field, ρ is the fluid density, $\nu_{\text{eff}} = \nu + \nu_t$ is the effective viscosity that is calculated as the sum of kinematic viscosity and turbulent eddy viscosity, c is a coefficient to flexibly control the strength of the added force field, and $\boldsymbol{a}$ is the Liutex-based force field source term to be constructed.

The eddy viscosity ν_t is obtained via the k-ω shear stress transport (SST) DDES model which is a hybrid RANS-LES model. The switching between Reynolds averaged Navier-Stokes (RANS) and LES is controlled by a modified turbulent length scale, which is defined as the minimum of the calculated length scale from RANS model and the local grid scale[21]

$$l_{\text{DDES}} = l_{\text{RANS}} - f_d \max(0, l_{\text{RANS}} - C_{\text{DES}}\Delta) \tag{2}$$

in which f_d is a "delay" function to protect the boundary from earlier separation and C_{DES} is an empirical coefficient called DES constant. Details about the formula of the functions and the values of the constant coefficients can be referred to Gritskevich et al.[22].

The source term $\boldsymbol{a}$ is given by a centripetal acceleration formula, as follows

$$\boldsymbol{a} = \frac{\boldsymbol{R}}{2}\times\left(\frac{\boldsymbol{R}}{2}\times\boldsymbol{l}\right) = \frac{1}{4}\boldsymbol{R}\times(\boldsymbol{R}\times\boldsymbol{l}) \tag{3}$$

$\boldsymbol{R}/2$ is half of the Liutex vector, representing the rigid rotational speed of the local fluid element, $\boldsymbol{l}$ is a length scale calculated by $\boldsymbol{l} = (\nabla\boldsymbol{u})^{-1}\cdot\boldsymbol{u}$ [15].

2. Flow past a three-dimensional cylinder without force field model

In this section, we first validate our numerical methods without force field model by comparing flow parameters with experimental results. The aspect ratio (length over diameter) of the circular cylinder is π. The coordinate origin is located at the center of the cylinder. The x-axis is pointing to the inflow direction, y-axis and z-axis are streamwise and spanwise directions, respectively. The computational domain extends from $-10D$ to $20D$ in x-direction, from $-10D$ to $10D$ in y-direction, and from $-\pi/D$ to π/D in z-direction, as shown in Fig. 1. This is large enough to eliminate the boundary reflection effect[23]. The O-type grid layout are adopted, as shown in Fig. 2. In order to resolve the sub-viscous boundary layer, the first layer thickness is ensured to correspond to a y^+ less than 1. The overall cell numbers of the mesh is 849 000.

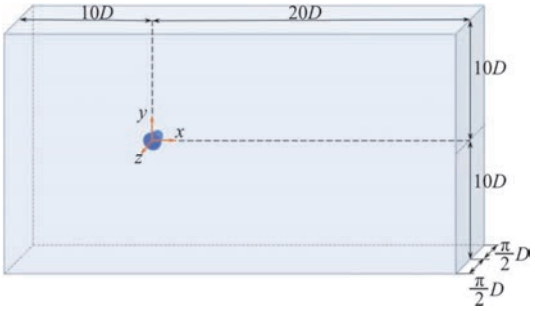

Fig. 1 (Color online) Computational domain of flow past a three-dimensional circular cylinder

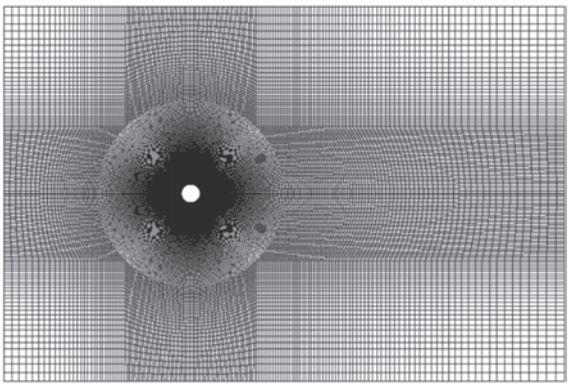

Fig. 2 Computational mesh of flow past a three-dimensional circular cylinder

Table 1 lists the flow quantities comparison between the present study and previous published experimental and numerical data. After removing the initial transient shedding cycles, the statistics are computed over 60 cycles to reach fully convergence and additional averaging is performed in the spanwise direction. As it can be seen from the table, the global quantities such as mean drag coefficient, Strouhal number, flow separation angle and mean base pressure coefficient are well predicted and are in good agreement with experiment.

Table 1 Overview of statistical flow parameters

Data	$C_{d,\mathrm{ave}}$	St	θ_{sep} /°	$-C_{pb}$
Exp.[19, 24]	0.98±0.05	0.215±0.005	85±2	0.90±0.05
DNS[16]	1.03	0.22	85.7	0.92
LES[18-19]	1.04	0.21	88	0.94
Present	0.985	0.213	86.02	0.858

3. Results and discussions

3.1 *The control regions*

The centripetal force model is not applied to the whole computational domain. Instead, it is activated inside a control region (CR) with rectangular shape. We first studied the influence of different CR location to find out the most influenced CR location. A graphical sketch in Fig. 3 shows the CR locations. We set up six different locations for comparison, marked as CR-A to CR-F. The x coordinate of left-most side of these CRs varies from $-1.5D$ to $4D$ Details of the locations for each CR are listed in Table 2. CR-A contains the front half side of the cylinder and CR-B contains the rear half side. The remaining CRs locate behind the cylinder with increasing distance away from the cylinder.

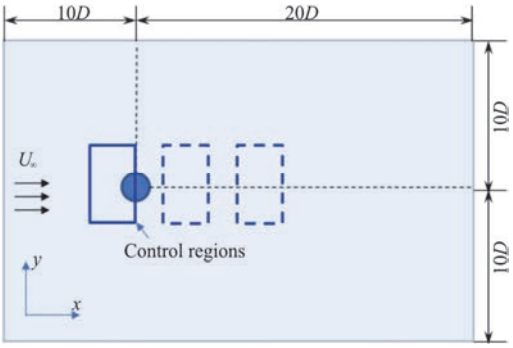

Fig. 3 (Color online) A graphical sketch of the control regions inside which the source term is applied

Table 2 The locations of left-most side for different CRs

CR	Locations
CR-A	$-1.5D$
CR-B	0
CR-C	$1D$
CR-D	$2D$
CR-E	$3D$
CR-F	$4D$

The centripetal force model is added to the flow field, with a positive source term coefficient $c = 1$. The time-averaged mean drag, root mean squared (rms) lift and Strouhal number of different CRs are compared and presented in Fig. 4 and Table 3. The solid lines represent the results from the original simulations without centripetal force model. For CR-A case in which the CR covers the front half of the cylinder, the drag and lift of the cylinder are slightly increasing. While the Strouhal number keeps almost invariance. Starting from CR-B, as the CR's location away from the cylinder, the drag and lift will first decrease to a minimum value at CR-C, and then become larger as the CR away from the cylinder. According to our previous study[15], the centripetal force field model with positive coefficient $(c > 0)$ will provide a driving force to negate the local rotational motion of the fluid and weaken the vortex strength. For case CR-B in which the CR wraps the rear half of the cylinder, since the vortical structures in CR are suppressed, the pressure drop at two sides of the cylinder will decrease. This explains why the lift force on the cylinder decreases when the centripetal force model is activated with $c > 0$. Counter-intuitively, the lift in case CR-C is even smaller than case CR-B, which means the vortices in CR-C is dominant flow structures accounting for the hydrodynamic forces exerting on the cylinder.

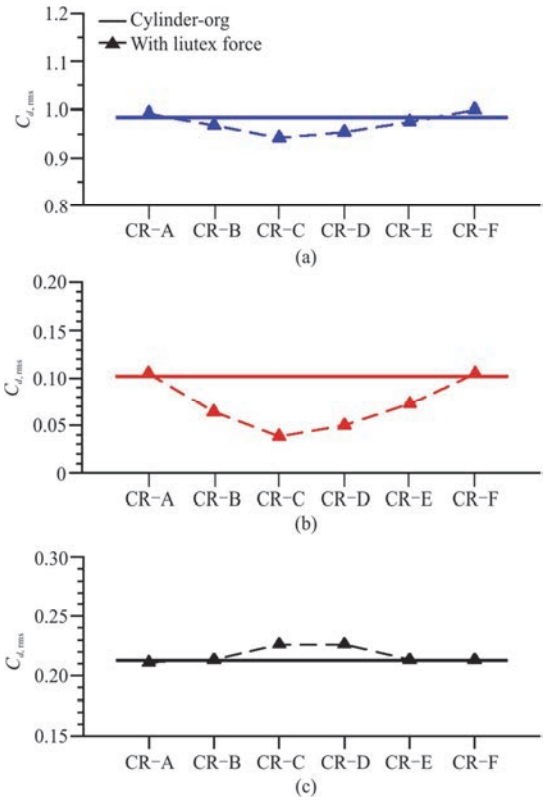

Fig. 4 (Color online) The variation of time-averaged drag coefficient, fluctuating lift coefficient and Strouhal number for cases with different CRs

Figure 5 shows the time-averaged mean surface pressure and wall shear stress distribution around the cylinder. The horizontal axis is the angle between the

Table 3 Flow quantities of the cylinder flow for different CRs

	c	$C_{d,\mathrm{ave}}$	$C_{l,\mathrm{rms}}$	St	θ_{sep} /°	$-C_{pb}$
Org	0	0.985	0.102	0.213	86.02°	0.858
A	1	0.992	0.105	0.211	-	-
B	1	0.968	0.064	0.214	85.59°	0.798
C	1	0.942	0.038	0.226	85.18°	0.770
D	1	0.954	0.050	0.226	85.13°	0.770
E	1	0.975	0.073	0.213	85.64°	0.820
F	1	0.990	0.105	0.213	85.97°	0.852

x-axis and the radial line through surface point. Zero degree is located at the stagnation point in front of the cylinder. The pressure and wall shear stress are nondimensionalized by the following formula

$$C_p = \frac{p - p_0}{0.5\rho U^2} \tag{4}$$

$$\tau = \frac{\tau_0}{\rho U^2}\sqrt{Re} \tag{5}$$

It has been observed that the surface pressure of

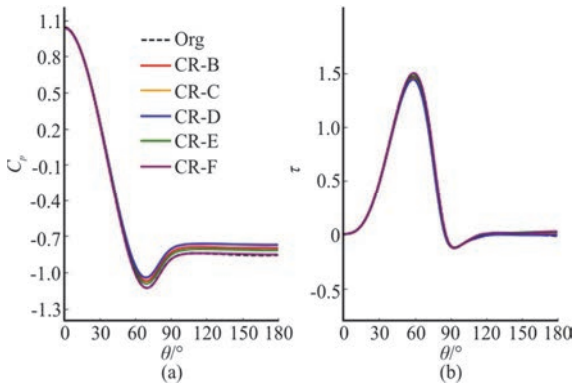

Fig. 5 (Color online) The time-averaged surface pressure (a) and wall shear stress (b) around the circular cylinder at the mid-plane

CR-C and CR-D are almost identical. These two CRs give the smallest surface pressure on the back surface of the cylinder. The base pressure coefficient decreases from 0.858 to 0.77 with about 10.3 percent reduction. The surface pressure of CR-F is slightly different from the original uncontrolled case, implying that for $c = 1$, when the distance between cylinder and CR is larger than $4D$, the effect of force field model on the surface pressure is trivial and can be neglected.

Since the CR-C case gives the most notable changes of drag, lift and vortex shedding frequency compared with the uncontrolled case, this CR is selected for subsequent studies of the source term strength.

3.2 *The effect of source term strength*

Based on the CR sensitivity studies in previous section, case CR-C is used for study the effect of different source term coefficients on the force and flow field of the cylinder. Four different source term strength including both positive and negative coefficients are considered. The statistically computed flow quantities such as time-averaged drag and root mean squared lift coefficients, Strouhal number, separation angle, base pressure coefficient, recirculation length and non-dimensional minimum streamwise velocity are listed in Table 4.

According to Bearman[25], the mean recirculation lengths are inversely proportional to the mean base

Table 4 Statistical flow quantities of the cylinder flow for different source term coefficients

Case No.	c	$C_{d,\mathrm{ave}}$	$C_{l,\mathrm{rms}}$	St	θ_{sep} /°	$-C_{pb}$	L_{rec}/D	$U_{\min}/U$
Org	0	0.985	0.102	0.213	86.02°	0.858	1.541	–0.291
Case P1	1	0.942	0.038	0.2262	85.18°	0.770	1.952	–0.266
Case P2	2	0.929	0.028	0.2276	84.58°	0.718	1.952	–0.255
Case M1	–1	1.168	0.418	0.1963	88.03°	1.020	0.927	–0.209
Case M2	–2	1.192	0.478	0.1885	88.44°	1.070	0.927	–0.222

pressure coefficients, and the mean drag coefficients are proportional to the mean base pressure coefficients. These rules could help understand the relationships in Table 4. Compared with the original case, it is obvious that there are negative correlations between coefficient c and drag/lift forces. Positive coefficient c in cases P1 and P2 give smaller mean drag and fluctuate lift forces than the original case. While for negative coefficient c in cases M1 and M2, both the drag and lift will increase. Considering a positive coefficient in the centripetal force model, it will resist the local rotation of fluid element, hence decrease the rotational velocity in vortex core region. This will further results in a smaller differential pressure between front and rear, left and right side of the cylinder hence gives a smaller drag and lift.

On the contrary, the Strouhal number's change tendency is opposite to drag and lift forces. The flow cases with positive coefficient will give a larger Strouhal number, which means a larger shedding frequency. The positive source term coefficient will suppress the alternate vortex shedding in two sides of the cylinder and the flow separation point will moving forward to the stagnation point. Consequently, the separation angle becomes smaller with positive coefficient. The time of flow from stagnation point to separation point is also reduced, results in a smaller shedding period and larger Strouhal number.

Figure 6 shows the time-averaged surface pressure coefficients and the nondimensionalized wall shear stress around the cylinder in the mid-plane for different coefficients. All the case share similar tendency in the front part of the cylinder ($\theta = 40°$) and become different even before flow separation. It is worth noting that for cases with negative coefficient, the surface pressure and wall shear stress difference are trivial until $\theta > 120°$. For case M2, the surface pressure continue decreasing and finally reaches −1.07 at the back pressure point.

Figure 7 illustrates the time-averaged streamwise velocity profile along the x-axis in the cylinder wake region. The streamwise velocity is negative in the recirculation zone, and restore to a positive value away from the cylinder. Velocity profiles are slightly different between coefficients with same sign, e.g., between $c = -1$ and $c = -2$. For negative coefficient, the centripetal force model will accelerate the rotational speed of local flow motion and form a stronger and larger recirculation zone. The recirculation length and the magnitude of minimum recirculation velocity are hence larger in the recirculation zone. In the far wake region, the restored streamwise velocity for $c > 0$ case is almost the same as uncontrolled case. However, that value is smaller for $c < 0$ cases, indicating that the strengthening of vortices with negative c will evolve to the far wake region.

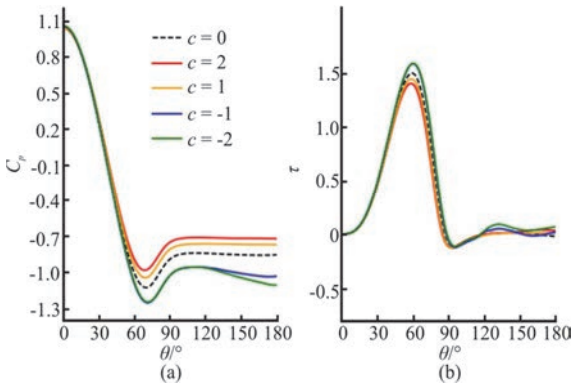

Fig. 6 (Color online) The time-averaged surface pressure (a) and wall shear stress (b) around the circular cylinder in the mid-plane for different source term coefficients

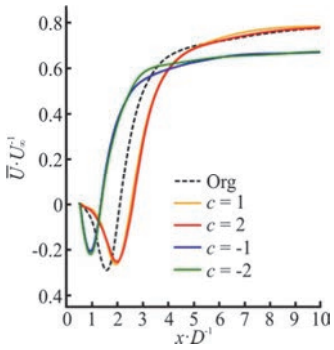

Fig. 7 (Color online) The time-averaged streamwise velocity profile along the x-axis in the cylinder wake region

Figure 8 gives the instantaneous three dimensional vortical structures of the cylinder flow in the wake regions for all the five different cases. The vortices are extracted by $\Omega_R = 0.52$ iso-surfaces with the modified Liutex-Omega method[12, 15]. The recirculation zone length cases with negative coefficients is obviously smaller. For cases with negative coefficients, the vortical structures are expanding in the cross flow direction and become wider, which is the outcome of vortex strengthening induced by force field model.

Figures 9, 10 show the instantaneous streamwise and cross-flow velocity profile in the wake of the circular cylinder, respectively. The three figures are contoured by the same level, i.e., 100 contours of non-dimensional (by free stream velocity) velocity component from −1.5 to 1.5. The black thick lines represent the zero value of the contours. The change tendency of recirculation bubble length are clearly seen in Fig. 9. And the Karman vortex street are vividly illustrated in Fig. 10. For case P2 which applies a positive source term, the vortices in the wake

region are squashed and the distance between vortex pairs are smaller. While for case M2 with a negative c, the vortices are stretched and the distance between vortex pairs are larger.

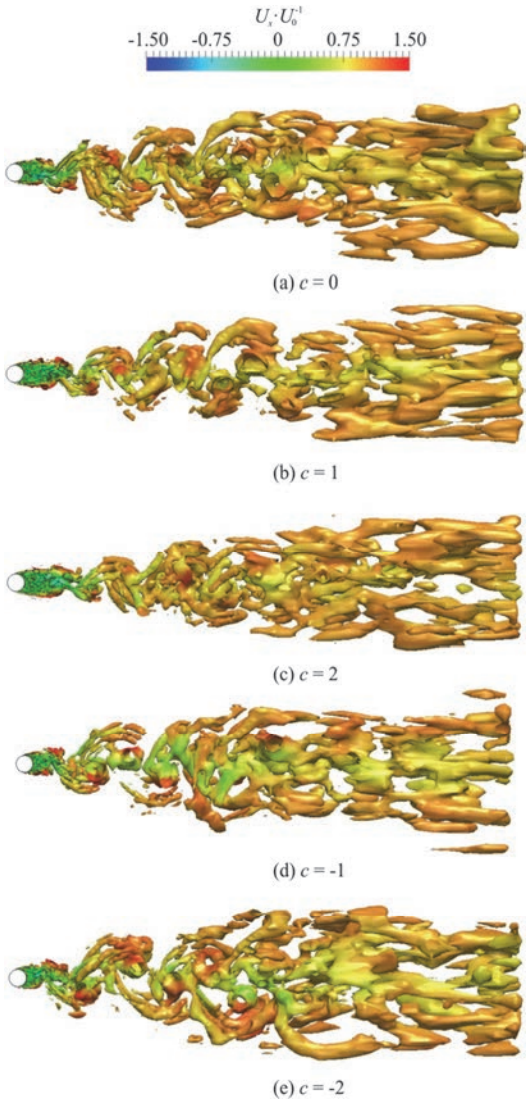

Fig. 8 (Color online) Instantaneous vortical structures in the cylinder wake region by the nondimensional $\Omega_R = 0.52$ iso-surfaces

The Liutex-Omega iso-surfaces are shown in Fig. 11 from both side and perspective views. The wake are strongly three-dimensional for all cases. For the $c = -2$ case, the strengthening of vortices will form a strong suction behind the cylinder, which moves the primary vortex formation and shedding closer to the cylinder, thus resulting in a narrower wake and is associated with a lower effective Reynolds number. This in turn generates a homogeneous distribution of instantaneous cylinder surface pressure along the spanwise direction, resulting in high levels of rms value for lift coefficient.

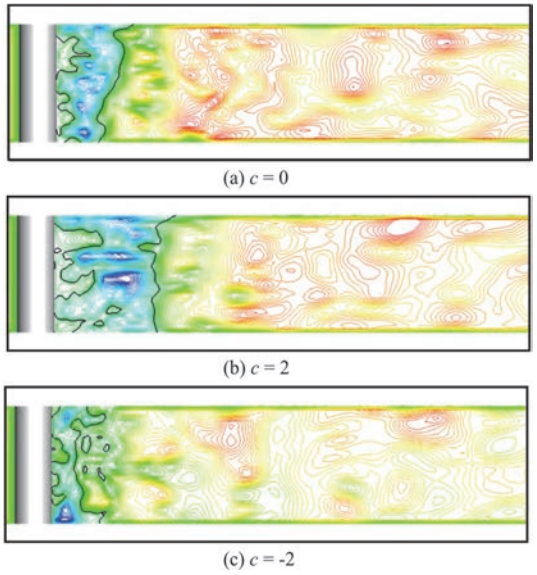

Fig. 9 (Color online) Instantaneous streamwise velocity profile in $y = 0$ plane in the wake of cylinder

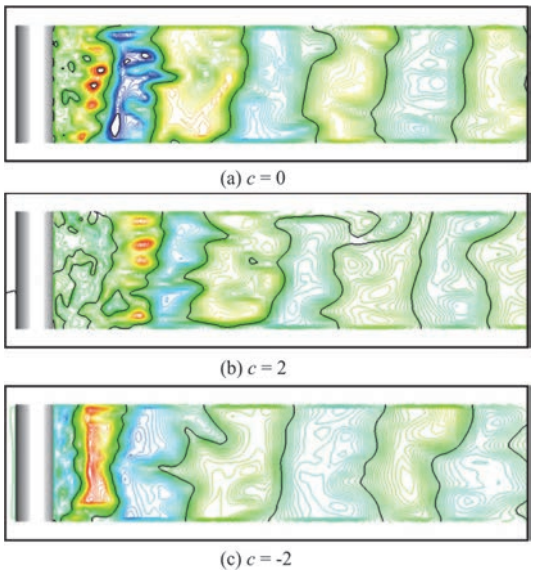

Fig. 10 (Color online) Instantaneous cross-flow velocity profile in $y = 0$ plane in the wake of cylinder

4. Conclusion

In this paper, the Liutex-based centripetal force field model is applied to the three dimensional turbulent flow past a circular cylinder at $Re = 3\,900$. The force field model is achieved by inserting a source term at the right hand side of the momentum equations. Turbulent flows around the circular cylinder are modeled by the delayed detached-eddy simulations based on the two-equation k-ω SST model. Prior to the simulation with force field model, the cylinder flow without force field model is simula-

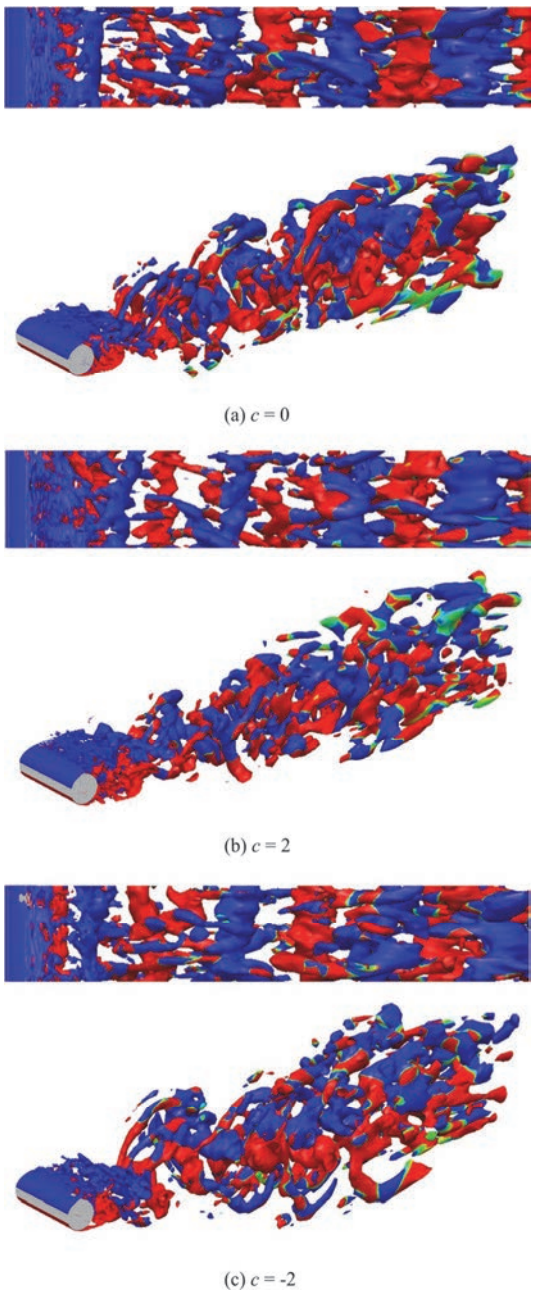

Fig. 11 (Color online) Instantaneous cross-flow velocity profile in $y = 0$ plane in the wake of cylinder

ted at first in order to validate the present numerical model. The statistical flow quantities such as mean drag coefficient, Strouhal number, separation angle and base pressure coefficient are in good agreement with previous experimental data. For a control region with certain size $(1.5D \times 2.4D)$, the impacts on hydrodynamic forces of different region locations are huge. Counterintuitively, it's the control region with some extent away from the cylinder downstream which gives the most influence on hydrodynamic forces and shedding frequency change. Based on this control region, parametric study on the source term strength is conducted. It is concluded that by changing the force field strength, the drag and lift show a negative correlations with respect to the source term coefficient c. Particularly, when $c = 2$ and -2, the reduction and increment of lift force are −72.5% and 369%, respectively. This shows effective change of hydrodynamic performance by vortex manipulation which can be used for structural design in the future and provide a new direction for performance improvement and optimization.

References

[1] Cao L. S., Huang F. L., Liu C. et al. Vortical structures and wakes of a sphere in homogeneous and density stratified fluid [J]. *Journal of Hydrodynamics*. 2021, 33(2): 207-215.

[2] Liu C., Gao Y. S., Dong X. R. et al. Third generation of vortex identification methods: Omega and Liutex/Rortex based systems [J]. *Journal of Hydrodynamics*, 2019, 31(2): 205-223.

[3] Hunt J. C. R., Wray A. A., Moin P. Eddies, streams, and convergence zones in turbulent flows [R]. Proceedings of the Summer Program. Center for Turbulence Research Report CTR-S88, 1988, 193-208.

[4] Jeong J., Hussain F. On the identification of a vortex [J]. *Journal of Fluid Mechanics*, 1995, 285: 69-94.

[5] Chong M. S., Perry A. E., Cantwell B. J. A general classification of three-dimensional flow fields [J]. *Physics of Fluids A: Fluid Dynamics*, 1990, 2(5): 765-777.

[6] Zhou J., Adrian R. J., Balachandar S., et al. Mechanisms for generating coherent packets of hairpin vortices in channel flow [J]. *Journal of Fluid Mechanics*, 1999, 387: 353-396.

[7] Epps B. Review of vortex identification methods [C]. *Proceedings of the 55th AIAA Aerospace Sciences Meeting*, Grapevine, Texas, USA, 2017.

[8] Liu C., Gao Y., Tian S. et al. Rortex–A new vortex vector definition and vorticity tensor and vector decompositions [J]. *Physics of Fluids*. 2018, 30(3): 035103.

[9] Gao Y., Liu C. Rortex and comparison with eigenvalue-based vortex identification criteria [J]. *Physics of Fluids*, 2018, 30(8): 085107.

[10] Liu J., Gao Y., Liu C. An objective version of the Rortex vector for vortex identification [J]. *Physics of Fluids*, 2019, 31(6): 065112.

[11] Dong X., Gao Y., Liu C. New normalized Rortex/vortex identification method [J]. *Physics of Fluids*, 2019, 31(1): 011701.

[12] Liu J., Liu C. Modified normalized Rortex/vortex identification method [J]. *Physics of Fluids*, 2019, 31(6): 061704.

[13] Gao Y. S., Liu J. M., Yu Y. et al. A Liutex based definition and identification of vortex core center lines [J]. *Journal of Hydrodynamics*, 2019, 31(3): 445-454.

[14] Yu H. D., Wang Y. Q. Liutex-based vortex dynamics: A preliminary study [J]. *Journal of Hydrodynamics*, 2020, 32(6): 1217-1220.

[15] Zhao W. W., Wang Y. Q., Chen S. T. et al. Parametric study of Liutex-based force field models [J]. *Journal of Hydrodynamics*. 2021, 33(1): 86-92.

[16] Ma X., Karamanos G. S., Karniadakis G. E. Dynamics and low-dimensionality of a turbulent near wake [J]. *Journal of Fluid Mechanics*, 2000, 410: 29-65.
[17] Mittal R., Moin P. Suitability of upwind-biased finite difference schemes for large-eddy simulation of turbulent flows [J]. *AIAA Journal*, 1997, 35(8): 1415-1417.
[18] Kravchenko A. G., Moin P. Numerical studies of flow over a circular cylinder at Re_D=3900 [J]. *Physics of Fluids*, 2000, 12(2): 403-417.
[19] Parnaudeau P., Carlier J., Heitz D. et al. Experimental and numerical studies of the flow over a circular cylinder at Reynolds number 3900 [J]. *Physics of Fluids*, 2008, 20(8): 085101.
[20] Lysenko D. A., Ertesvåg I. S., Rian K. E. Large-eddy simulation of the flow over a circular cylinder at Reynolds number 3900 using the OpenFOAM toolbox [J]. *Flow, Turbulence and Combustion*, 2012, 89(4): 491-518.
[21] Zhao W. W., Wan D. C. Detached-eddy simulation of flow past tandem cylinders [J]. *Applied Mathematics and Mechanics (Engilsh Edition)*, 2016, 37(12): 1272-1281.
[22] Gritskevich M. S., Garbaruk A. V., Schütze J. et al. Development of DDES and IDDES formulations for the *k-ω* shear stress transport model [J]. *Flow, Turbulence and Combustion*, 2012, 88(3): 431-449.
[23] Travin A., Shur M., Strelets M. et al. Detached-eddy simulations past a circular cylinder [J]. *Flow, Turbulence and Combustion*, 2000, 63(1-4): 293-313.
[24] Norberg C. An experimental investigation of the flow around a circular cylinder: influence of aspect ratio [J]. *Journal of Fluid Mechanics*, 1994, 258: 287-316.
[25] Bearman P. W. Investigation of the flow behind a two-dimensional model with a blunt trailing edge and fitted with splitter plates [J]. *Journal of Fluid Mechanics*, 1965, 21(2): 241-255.